

Received 11 May 2021; revised 11 June 2021; accepted 27 June 2021. Date of publication 2 July 2021; date of current version 14 July 2021.
The review of this article was arranged by Editor A. G. U. Perera.

Digital Object Identifier 10.1109/JEDS.2021.3094281

Self-Aligned Top-Gate Amorphous Zinc-Tin Oxide Thin-Film Transistor With Source/Drain Regions Doped by Al Reaction

HUAN YANG¹, JIYE LI¹, XIAOLIANG ZHOU¹, LEI LU¹,
AND SHENG DONG ZHANG^{1,2} (Senior Member, IEEE)

¹ School of Electronic and Computer Engineering, Peking University, Shenzhen 518055, China

² School of Electronics Engineering and Computer Science, Peking University, Beijing 100871, China

CORRESPONDING AUTHOR: S. ZHANG (e-mail: zhangsd@pku.edu.cn)

This work was supported in part by the National Natural Science Foundation of China under Project 61774010; and in part by the Shenzhen

Municipal Scientific Program under Grant JCYJ20180504165449640, Grant JCYJ20200109140610435, and Grant XMHT20190201013.

ABSTRACT A self-aligned fabrication process for top-gate amorphous zinc-tin oxide (a-ZTO) thin-film transistors (TFTs) is developed, in which the source/drain (S/D) doping is realized through depositing a thin aluminum (Al) film on S/D regions and performing a thermal annealing. Results indicate that a chemical oxidation-reduction reaction between Al and a-ZTO films takes place during the thermal annealing process, and shallow donors of oxygen vacancies and metal tin (Sn) interstitials are thus generated. The formed S/D regions have a high carrier concentration over $1 \times 10^{20} \text{ cm}^{-3}$, low sheet resistance of $0.57 \text{ k}\Omega/\text{sq}$, and high thermal stability even in oxygen ambient. The fabricated a-ZTO TFTs exhibit excellent electrical performances, including a low channel-width-normalized S/D resistance of about $7.05 \text{ }\Omega \text{ cm}$, a high field-effect mobility of $15.7 \text{ cm}^2/\text{Vs}$, a high on/off current ratio of over 10^8 , and near-zero turn-on voltage. Moreover, good electrical stability with less than 0.2-V threshold voltage shift under $\pm 30\text{-V}$ gate bias stresses is also achieved.

INDEX TERMS Amorphous zinc-tin oxide, self-aligned top-gate, thin-film transistor, Al reaction doping, oxidation-reduction reaction.

I. INTRODUCTION

Amorphous metal oxide semiconductors (AOS) thin-film transistors (TFTs) have been demonstrated to have relatively high carrier mobility, good performance uniformity over large-area, and low fabrication cost, and thereby regarded as one of the most promising devices applicable to advanced large area electronics and high-end integrated circuits [1]–[9]. The high mobility of AOS TFTs is usually attributed to the heavy metal cations, such as indium (In), which have an electronic configuration of $(n-1)d^{10} ns^0$ ($n \geq 5$) allowing large-radius spherical s orbitals and sufficient orbital overlapping [6]–[8]. As a result, the superiorities of the In-based AOS TFTs, like amorphous indium-gallium-zinc oxide (a-IGZO) [5]–[8] and amorphous indium-zinc oxide (a-IZO) [8]–[11] have earned them popularity in various applications. Unfortunately, In is toxic and

short of reserve in earth [5], [12], [13]. On the other hand, the metal tin (Sn) is safe and abundant [12], [13], and has the similar electronic configuration [8] and close coordination number [14] to indium in an amorphous oxide system. Thus, the In-free amorphous zinc-tin oxide (a-ZTO) has been investigated as a promising non-toxic low-cost AOS, and reasonably high performance and stability of a-ZTO TFTs have also been well demonstrated in recent years [12], [15]–[22].

Among various AOS TFT structures, the bottom-gate one is not suitable for advanced systems requiring high integration density due to the large footprint, parasitic capacitance and poor scalability imposed by the large overlap between metallic source/drain (S/D) and gate electrode [10], [12], [22]. In contrast, the top-gate (TG) architecture with self-aligned (SA) S/D is ideal for ultrahigh-resolution displays, BEOL transistors and other high-end

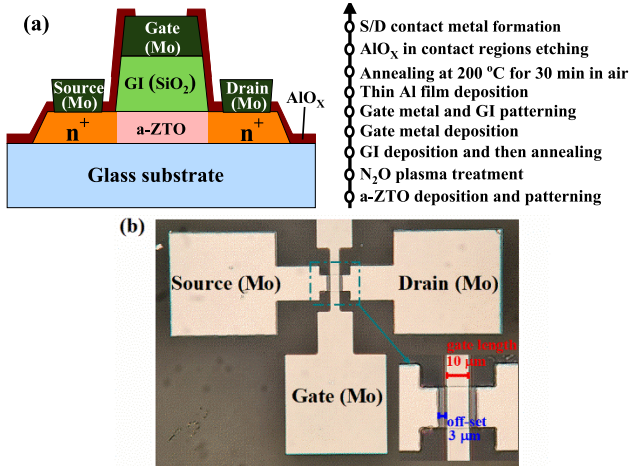


FIGURE 1. (a) Schematic cross-section view and the major fabrication process and (b) top view of the SATG a-ZTO TFT with Al reaction doped S/D regions.

applications. The vital SA formation of the n⁺ S/D with the TG a-ZTO TFTs has been successfully implemented using Ar [12] and NF₃ [22] plasma treatment. However, the plasma induced low resistance of AOS tends to be readily returned to the high-resistance state in subsequent post-annealing treatments in an oxidizing ambient [10], [23], [24]. Recently, it has been reported that the aluminum (Al) reaction is an effective and stable S/D doping method for fabrication of SATG a-IZO and a-IGZO TFTs [10], [23]–[26]. And, the Al reaction with a-ZTO films has also been investigated [27]. To date, however, the Al reaction doping method for fabrication of SATG a-ZTO TFTs has not been studied yet.

In this work, a SATG a-ZTO TFT fabrication process is developed, in which the n⁺ S/D doping is performed using the metal Al reaction method. High performance of SATG a-ZTO TFTs with low and stable S/D resistance are fabricated with this process. The applicability of the Al reacted S/D doping method for fabrication of TG a-ZTO TFTs is demonstrated well.

II. EXPERIMENTAL DETAILS

Fig. 1 shows the schematic cross-sectional view and the main fabrication process flow of the SATG a-ZTO TFTs with S/D doped using Al reaction. Firstly, the a-ZTO film with 40 nm in thickness was sputtered on the glass substrate by using a ZnSnO ceramic target with Zn:Sn = 2:1 in atomic ratio. The work gas in the sputtering process was the mixture of Ar and oxygen (O₂) with a flow rate ratio of 48:2. Following the a-ZTO island patterning in diluted hydrochloric acid, the gate insulator (GI) of 200-nm-thick silicon oxide (SiO₂) was grown by plasma-enhanced chemical vapor deposition (PECVD), right after the nitrous oxide (N₂O) plasma treatment for 200 s. Next, the samples were annealed at 400 °C in O₂ ambient for 60 min. Following that, the molybdenum (Mo) film was deposited as the gate

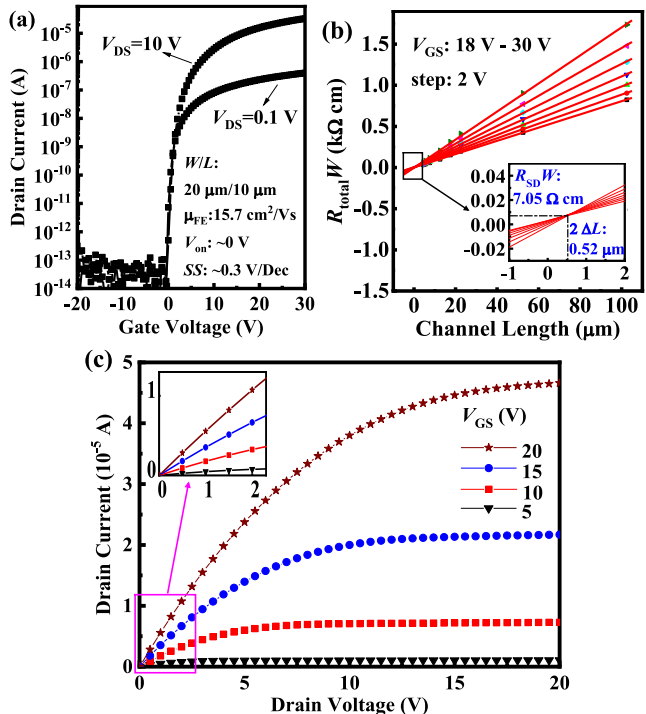


FIGURE 2. (a) Transfer curves of SATG a-ZTO TFT with Al reaction treated S/D regions. (b) Channel width-normalized total resistance (R_{total} W) of the fabricated TFTs biased at various gate voltages versus channel length. (c) Output curves of the fabricated TFT.

electrode, and Mo and GI were patterned to form the gate electrode and expose the a-ZTO in S/D regions.

Then, Al reaction doping process was conducted to form the n⁺-a-ZTO S/D regions. A thin Al film with thickness about 5 nm was sputtered first, followed by annealing at 200 °C in air for 30 min. Finally, 100-nm-thick Mo film was sputtered and patterned using lift-off process to form S/D contact electrodes. The AlO_x film in the contact regions generated during the Al reaction process was removed using diluted tetramethylammonium hydroxide (2.38% TMAH) before the contact metal deposition. Fig. 1(b) shows the top view of the fabricated TFT. The electrical characteristics of the fabricated a-ZTO films and TFTs were measured by an Agilent B1500 semiconductor parameter analyzer in dark ambient environment. X-ray photoelectron spectroscopy (XPS) analysis was performed by using a Thermo Fisher ESCALAB 250X interface analysis system equipped with a monochromatized Al anode X-ray source ($\hbar\nu = 1486.6$ eV). Hall effect measurement was conducted using an HMS-3000.

III. RESULTS AND DISCUSSION

Fig. 2(a) shows transfer curves of the Al reaction-treated SATG a-ZTO TFT with channel width (W) of 20 μm and length (L) of 10 μm. The drain currents versus gate voltages were measured at drain to source voltages (V_{DS}) of 0.1 V and 10 V. As shown, with the Al reaction doped S/D, the a-ZTO TFT exhibits excellent comprehensive performances, such as a relatively high field-effect mobility

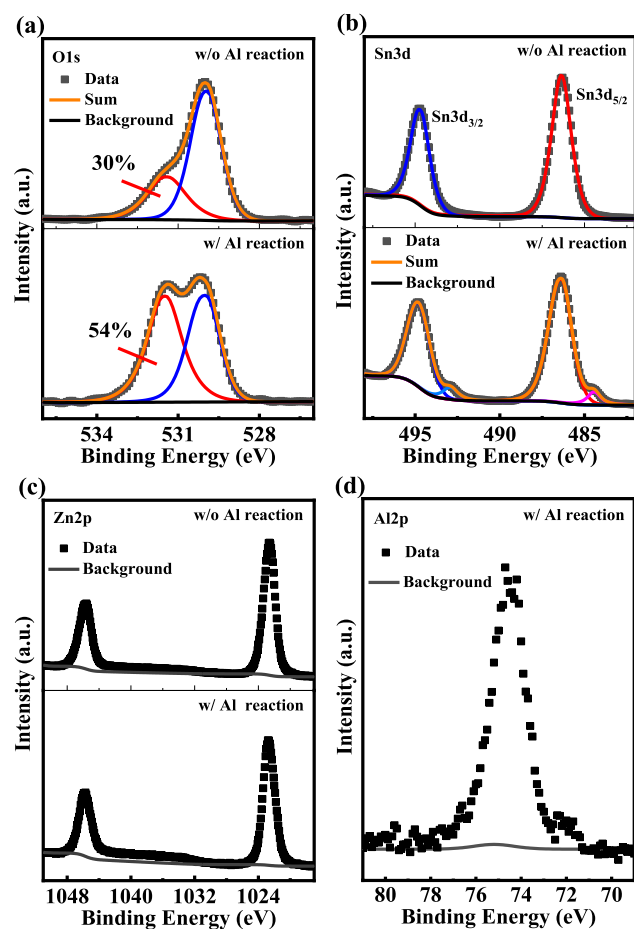
TABLE 1. Comparision of the effect of different doping processes on ZTO.

Doping process	ZTO thickness (nm)	R_{sheet} (k Ω /sq)	Carrier Conc. (cm^{-3})	Hall Mobi. (cm^2/Vs)	Ref.
w/o Al reaction	40	$> 1 \times 10^7$	$< 1 \times 10^{13}$	~ 13	This work
Ar plasma	40	0.57	1.22×10^{20}	22.36	This work
NF ₃ plasma	25	1.9	-	22	[22]

(μ_{FE}) of $15.7 \text{ cm}^2/\text{Vs}$, a high on/off current ratio over 10^8 , a near-zero turn-on voltage (V_{on}) and a decent subthreshold slope (SS) of $\sim 0.3 \text{ V/dec}$. Fig. 2(b) shows the L -dependent W -normalized total resistance ($R_{\text{total}}W$) of the fabricated SATG a-ZTO TFT biased at various gate voltages. The W -normalized S/D resistance ($R_{\text{SD}}W$) of the Al-reacted S/D was extracted by using transfer length method (TLM) to be $7.05 \Omega\text{cm}$ and much lower than that of the plasma treated-S/D [12]. The extracted sub-micrometer L shrinking ($2 \Delta L = 0.52 \mu\text{m}$) suggests a minor lateral dopant diffusion from S/D into channel and thus explains the low channel carrier concentration reflected by the ideal V_{on} , benefiting from the low thermal budget of metal reaction. Fig. 2(c) shows the output characteristics of the fabricated TFTs. No current crowding effect is observed within the low drain voltage region, indicating that a perfect Ohmic contact between a-ZTO S/D and Mo electrodes, and a low enough series resistance in a-ZTO S/D regions were formed. The effectiveness of Al reaction method for doping S/D of SATG a-ZTO TFT is thus well confirmed.

Table 1 summarizes the sheet resistance (R_{sheet}), carrier concentration and Hall mobility of the Al reaction-doped a-ZTO, as well as those of the plasma-treated ones [12], [22]. As shown, R_{sheet} of Al reaction doped a-ZTO is $0.57 \text{ k}\Omega/\text{sq}$, much smaller than that of the plasma treated ones [12], [22]. Moreover, such a low resistance of the a-ZTO doped by Al reaction method is mainly attributed to the enormous increase in carrier concentration (about seven orders of magnitude), rather than the slight increase in Hall mobility, thus also enabling the perfect S/D Ohmic contact.

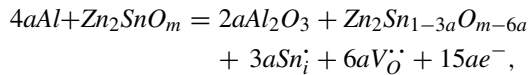
To clarify the carrier generation mechanism of the Al reaction process, chemical states of the critical elements in the a-ZTO films without and with Al reaction treatment were comparatively analyzed by XPS. Fig. 3(a)–3(c) respectively shows XPS spectra of the O 1s level, the Sn 3d level and the Zn 2p level. The O 1s peak shown in Fig. 3(a) can be deconvoluted into two subpeaks. The peak centered at the lower binding energy of $\sim 530.0 \text{ eV}$ (blue) is associated with the lattice oxygen in the M-O bond of a-ZTO system, while the other one centered at the higher binding energy of $\sim 531.4 \text{ eV}$ (red) is associated with the oxygen vacancy. As shown, with Al reaction treatment, the area percentage of the red subpeak increases from 30% to 54%. The result suggests that large amounts of oxygen vacancies be generated

**FIGURE 3.** XPS spectra of (a) O 1s level, (b) Sn 3d level and (c) Zn 2p level for a-ZTO films without and with Al reaction treatment. (d) XPS spectrum of Al 2p level for a-ZTO film with Al reaction treatment.

during the Al reaction process [26]–[28]. Regarding the Sn 3d signals shown in Fig. 3(b), in addition to the peaks centered at 494.7 eV for Sn 3d_{3/2} and 486.4 eV for Sn 3d_{5/2}, extra peaks centered at the lower binding energies (492.9 eV for Sn 3d_{3/2} and 484.4 eV for Sn 3d_{5/2}) are also observed for the Al reaction-doped a-ZTO, suggesting the formation of metallic Sn interstitials. This means the reduction of oxidation state of Sn element in the a-ZTO system, also consistent with the increase in oxygen vacancies shown in Fig. 3(a). However, as shown in Fig. 3(c), no obvious difference is seen in Zn 2p signals. Fig. 3(d) further shows XPS of Al 2p level of the Al-reacted a-ZTO film, where almost only the oxidation state can be found, suggesting a thorough oxidization of Al into AlO_X in the doping process.

It is thus inferred that an oxidation-reduction reaction between Al and a-ZTO system takes place in the doping process, much similar to what happens in the Al, titanium (Ti) or manganese (Mn) reaction-doped a-IGZO [26], [28], [29]. More specifically, Al elements react with Sn-O bonds of a-ZTO system as the Gibbs free energy of Al with Sn-O ($\Delta G = -539.2 \text{ kJ/mol}$ at 200°C) is lower than that of Al with Zn-O ($\Delta G = -207.4 \text{ kJ/mol}$ at 200°C). During the reaction, Al seizes oxygen from the Sn–O bonds of a-ZTO

system, like what Al, Ti or Mn does with the In-O bonds of a-IGZO [26], [28], [29], forming oxygen vacancies and simultaneously leaving the displaced Sn interstitials that act as shallow donors. Thus, the oxidation-reduction reaction could be described as



where the Sn_i^+ is the ionized Sn interstitial and V_O^- is the ionized oxygen vacancy.

In order to investigate the thermal stability of the fabricated SATG a-ZTO TFTs with n+ S/D formed by the Al reaction doping, a thermal anneal at 300 °C in O₂ was subjected to the devices with Ar plasma and Al reaction doped S/D regions, respectively. Fig. 4(a) and Fig. 4(b) respectively show the evaluations of transfer curves of these two devices with the anneal durations. After 5-min annealing, the transfer curves of the Ar plasma-treated SATG a-ZTO TFT exhibit a much lowered on-state current, indicating a remarkably increased R_{SD} . This is in consistence with the readily thermal annihilation of oxygen vacancies in the Ar plasma-treated n⁺ AOS [10], [23], [24]. In contrast, no noticeable change is seen in the transfer curves of the Al reaction-treated SATG a-ZTO TFT, revealing a better thermal stability. It is reasonably supposed that the good thermal stability originates from the reaction-generated AlO_X. The AlO_X film could isolate S/D regions from the O₂ during annealing, protecting the underneath oxygen vacancies or Sn interstitials from compensation or re-oxidation. To verify this, the same annealing process was conducted to the Al-reacted device with the AlO_X removed. As shown in Fig. 4(c), the transfer curves of the a-ZTO TFT indeed exhibit a much degraded on-state current, similar to what happens in the Ar plasma treated devices. Therefore, the AlO_X byproduct takes the credit of enhanced thermal stability of the Al-reacted SATG a-ZTO TFTs.

The electrical stability of the Al-reacted SATG a-ZTO TFTs was also evaluated. Figs. 5(a) and (b) show evolutions of the transfer curves under positive bias stress (PBS) and negative bias stress (NBS), respectively. It is seen that the devices exhibit a negligible threshold voltage shift (ΔV_{TH}) after being stressed for 3600-s under the PBS and NBS, respectively. It is thus believed that the Al reaction-doping process should not bring the a-ZTO TFTs additional defects which would worsen the electrical stability.

IV. CONCLUSION

A SATG a-ZTO TFT technology featuring Al reaction doping of S/D regions has been developed. The doped a-ZTO film exhibits a low resistivity with the carrier concentration higher than $1 \times 10^{20} \text{ cm}^{-3}$. The high concentration of carriers is experimentally verified to originate from the induced oxygen vacancies and metal Sn interstitials in the oxidation-reduction reaction between Al and a-ZTO system. The fabricated SATG a-ZTO TFTs with the proposed process exhibit high performance metrics, such as a high μ_{FE}

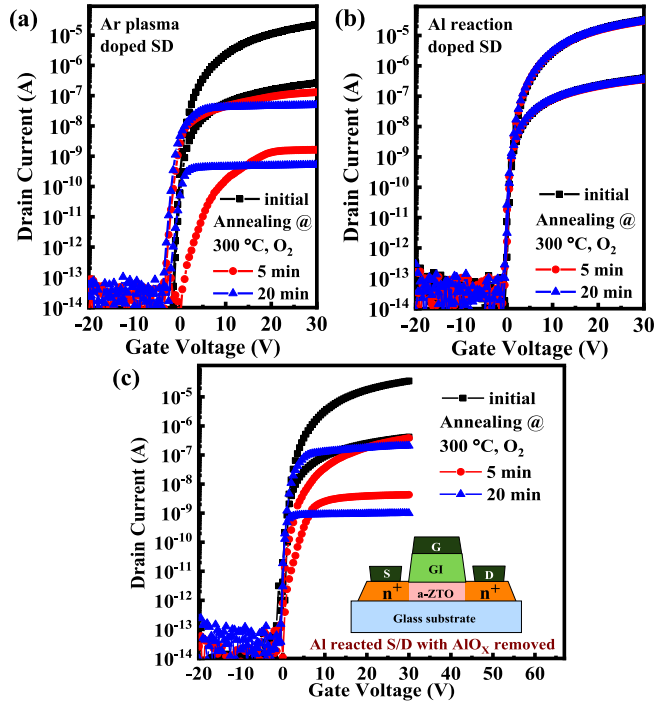


FIGURE 4. Transfer curve evolutions after O₂ anneal in (a) Ar plasma-, (b) Al reaction-treated SATG a-ZTO TFTs and (c) Al reaction-treated TFT with the generated AlO_X removed. The inset in Fig. 4(c) is schematic cross-section view of the Al reaction-treated TFT with the generated AlO_X removed.

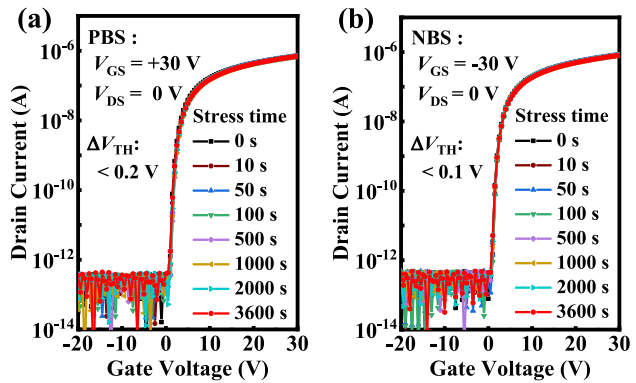


FIGURE 5. Time evolutions of transfer curves of the fabricated SATG a-ZTO TFTs with Al reaction doped S/D under (a) positive bias stress (PBS) and (b) negative bias stress (NBS).

of $15.7 \text{ cm}^2/\text{Vs}$, a high on/off current ratio over 10^8 , a near-zero V_{on} , a decent SS of $\sim 0.3 \text{ V/dec}$, and negligible ΔV_{TH} of less than 0.2 V under ± 30 -V gate bias stresses, benefiting from the low resistance of the Al-reacted a-ZTO S/D regions and the minor defect diffusion into channel. Moreover, the excellent oxygen-isolation effect of the by-produced AlO_X film ensures a good thermal stability.

ACKNOWLEDGMENT

This work was conducted in Shenzhen TFT and Advanced Display Lab.

REFERENCES

- [1] E. Fortunato, P. Barquinha, and R. Martins, "Oxide semiconductor thin film transistors: A review of recent advances," *Adv. Mater.*, vol. 24, no. 22, pp. 2945–2986, Jun. 2012, doi: [10.1002/adma.201103228](https://doi.org/10.1002/adma.201103228).
- [2] D. Ji *et al.*, "Recent progress in the development of backplane thin film transistors for information displays," *J. Inf. Display*, vol. 22, no. 1, pp. 1–11, Sep. 2020, doi: [10.1080/15980316.2020.1818641](https://doi.org/10.1080/15980316.2020.1818641).
- [3] M. Kimura, "Emerging applications using metal-oxide semiconductor thin-film devices," *Jpn. J. Appl. Phys.*, vol. 58, no. 9, pp. 1–10, Sep. 2019, doi: [10.7567/1347-4065/ab1868](https://doi.org/10.7567/1347-4065/ab1868).
- [4] M. Coll *et al.*, "Towards oxide electronics: A Roadmap," *Appl. Surf. Sci.*, vol. 482, pp. 1–93, Jul. 2019, doi: [10.1016/j.apsusc.2019.03.312](https://doi.org/10.1016/j.apsusc.2019.03.312).
- [5] J. Song, X. Huang, C. Han, Y. Yu, Y. Su, and P. Lai, "Recent developments of flexible InGaZnO thin-film transistor," *Phys. Status Solidi A*, vol. 218, no. 7, 2021, Art. no. 2000527, doi: [10.1002/pssa.202000527](https://doi.org/10.1002/pssa.202000527).
- [6] K. Nomura, H. Ohta, A. Takagi, T. Kamiya, M. Hirano, and H. Hosono, "Room-temperature fabrication of transparent flexible thin-film transistors using amorphous oxide semiconductors," *Nature*, vol. 432, no. 7016, pp. 488–492, Nov. 2004, doi: [10.1038/nature03090](https://doi.org/10.1038/nature03090).
- [7] H. Hosono, "Ionic amorphous oxide semiconductors: Material design, carrier transport, and device application," *J. Non-Cryst. Solids*, vol. 352, no. 2, pp. 851–858, Jun. 2006, doi: [10.1016/j.jnoncrysol.2006.01.073](https://doi.org/10.1016/j.jnoncrysol.2006.01.073).
- [8] J.-Y. Kwon, D.-J. Lee, and K.-B. Kim, "Review paper: Transparent amorphous oxide semiconductor thin film transistor," *Electron. Mater. Lett.*, vol. 7, no. 1, pp. 1–11, Mar. 2011, doi: [10.1007/s13391-011-0301-x](https://doi.org/10.1007/s13391-011-0301-x).
- [9] N. Itagaki *et al.*, "Zn-In-O based thin-film transistors: Compositional dependence," *Phys. Status Solidi A*, vol. 205, no. 8, pp. 1915–1919, 2008, doi: [10.1002/pssa.200778909](https://doi.org/10.1002/pssa.200778909).
- [10] T. Liang, Y. Shao, H. Lu, X. Zhou, X. Deng, and S. Zhang, "Scalability and stability enhancement in self-aligned top-gate indium-zinc-oxide TFTs with Al reacted source/drain," *IEEE J. Electron Devices Soc.*, vol. 6, pp. 680–684, 2018, doi: [10.1109/JEDS.2018.2837352](https://doi.org/10.1109/JEDS.2018.2837352).
- [11] E. Fortunato, P. Barquinha, A. Pimentel, L. Pereira, G. Gonçalves, and R. Martins, "Amorphous IZO TFTs with saturation mobilities exceeding 100 cm²/Vs," *Phys. Status Solidi RRL*, vol. 1, no. 1, pp. R34–R36, 2007, doi: [10.1002/pssr.200600049](https://doi.org/10.1002/pssr.200600049).
- [12] G. Wang *et al.*, "Implementation of self-aligned top-gate amorphous zinc tin oxide thin-film transistors," *IEEE Electron Device Lett.*, vol. 40, no. 6, pp. 901–904, Jun. 2019, doi: [10.1109/LED.2019.2910462](https://doi.org/10.1109/LED.2019.2910462).
- [13] R. Branquinho *et al.*, "Towards environmental friendly solution-based ZTO/AIO_x TFTs," *Semicond. Sci. Technol.*, vol. 30, no. 2, pp. 1–8, 2015, doi: [10.1088/0268-1242/30/2/024007](https://doi.org/10.1088/0268-1242/30/2/024007).
- [14] W. Körner, D. F. Urban, and C. Elsässer, "Generic origin of subgap states in transparent amorphous semiconductor oxides illustrated for the cases of In-Zn-O and In-Sn-O," *Phys. Status Solidi A*, vol. 212, no. 7, pp. 1476–1481, 2015, doi: [10.1002/pssa.201431871](https://doi.org/10.1002/pssa.201431871).
- [15] A. Liu *et al.*, "Redox chloride elimination reaction: Facile solution route for indium-free, low-voltage, and high-performance transistors," *Adv. Electron. Mater.*, vol. 3, no. 3, pp. 1–10, 2017, doi: [10.1002/aelm.201600513](https://doi.org/10.1002/aelm.201600513).
- [16] C. Fernandes *et al.*, "A Sustainable approach to flexible electronics with zinc-tin oxide thin-film transistors," *Adv. Electron. Mater.*, vol. 4, no. 7, pp. 1–10, Jul. 2018, doi: [10.1002/aelm.201800032](https://doi.org/10.1002/aelm.201800032).
- [17] H. Q. Chiang, J. F. Wager, and R. L. Hoffman, "High mobility transparent thin-film transistors with amorphous zinc tin oxide channel layer," *Appl. Phys. Lett.*, vol. 86, no. 1, pp. 1–3, 2005, doi: [10.1063/1.1843286](https://doi.org/10.1063/1.1843286).
- [18] H. W. Lee *et al.*, "Comprehensive studies on the carrier transporting property and photo-bias instability of sputtered zinc tin oxide thin film transistors," *IEEE Electron Device Lett.*, vol. 61 no. 9, pp. 3191–3198, Sep. 2014, doi: [10.1109/TED.2014.2337307](https://doi.org/10.1109/TED.2014.2337307).
- [19] P. Görn, M. Lehnhardt, T. Riedl, and W. Kowalsky, "The influence of visible light on transparent zinc tin oxide thin film transistors," *Appl. Phys. Lett.*, vol. 91, no. 19, 2007, Art. no. 193504, doi: [10.1063/1.2806934](https://doi.org/10.1063/1.2806934).
- [20] M. Fakhri, M. Theisen, A. Behrendt, P. Ge orrn, and T. Riedl, "Top-gate zinc tin oxide thin-film transistors with high bias and environmental stress stability," *Appl. Phys. Lett.*, vol. 104, no. 25, pp. 1–5, Jun. 2014, doi: [10.1063/1.4885362](https://doi.org/10.1063/1.4885362).
- [21] T. Riedl, P. Görn, P. Hölder, and W. Kowalsky, "Ultra-high long-term stability of oxide-TFTs under current stress," *Phys. Status Solidi RRL*, vol. 1, no. 5, pp. 175–177, 2007, doi: [10.1002/pssr.200701129](https://doi.org/10.1002/pssr.200701129).
- [22] Y. G. Kim, R. N. Bukke, J. Lee, J. K. Saha, and J. Jang, "Formation of F-doped offset region for spray pyrolyzed self-aligned coplanar amorphous zinc-tin-oxide thin-film transistor by NF₃ plasma treatment," *IEEE Trans. Electron Devices*, vol. 68, no. 3, pp. 1057–1062, Mar. 2021, doi: [10.1109/TED.2021.3051919](https://doi.org/10.1109/TED.2021.3051919).
- [23] N. Morosawa, Y. Ohshima, M. Morooka, T. Arai, and T. Sasaoka, "Novel self-aligned top-gate oxide TFT for AMOLED displays," *J. Soc. Inf. Display*, vol. 20, no. 1, pp. 47–52, 2012, doi: [10.1889/JSID20.1.47](https://doi.org/10.1889/JSID20.1.47).
- [24] Y. Shao *et al.*, "Homo-junction bottom-gate amorphous In-Ga-Zn-O TFTs with metal-induced source/drain regions," *IEEE J. Electron Devices Soc.*, vol. 7, pp. 52–56, 2019, doi: [10.1109/JEDS.2018.2876618](https://doi.org/10.1109/JEDS.2018.2876618).
- [25] T. Toda, G. Tatsuoka, Y. Magari, and M. Furuta, "High-performance top-gate and self-aligned In-Ga-Zn-O thin-film transistor using coatable organic insulators fabricated at 150 °C," *IEEE Electron Device Lett.*, vol. 37, no. 8, pp. 1006–1009, Aug. 2016, doi: [10.1109/LED.2016.2582319](https://doi.org/10.1109/LED.2016.2582319).
- [26] H. Yang *et al.*, "Metal reaction-induced bulk-doping effect in forming conductive source-drain regions of self-aligned top-gate amorphous InGaZnO thin-film transistors," *ACS Appl. Mater. Interfaces*, vol. 13, no. 9, pp. 11442–11448, Feb. 2021, doi: [10.1021/acsami.0c21123](https://doi.org/10.1021/acsami.0c21123).
- [27] S. Wang, B. Chang, and S. Zhang, "P-1.13: The conductivity modulation of amorphous zinc tin oxide thin film by aluminum (Al) reaction method," in *SID Symp. Dig. Tech. Papers*, vol. 50, Sep. 2019, pp. 673–676, doi: [10.1002/sdtp.13607](https://doi.org/10.1002/sdtp.13607).
- [28] M. E. Rivas-Aguilar *et al.*, "Specific contact resistance of IGZO thin film transistors with metallic and transparent conductive oxides electrodes and XPS study of the contact/semiconductor interfaces," *Current Appl. Phys.*, vol. 18, no. 7, pp. 834–842, 2018, doi: [10.1016/j.cap.2018.04.002](https://doi.org/10.1016/j.cap.2018.04.002).
- [29] P. S. Yun and J. Koike, "Metal reaction doping and ohmic contact with Cu-Mn electrode on amorphous In-Ga-Zn-O semiconductor," *J. Electrochem. Soc.*, vol. 158, no. 10, pp. H1034–H1040, Aug. 2011, doi: [10.1149/1.3621723](https://doi.org/10.1149/1.3621723).